LINK TO ONLINE ABSTRACT IN THE OSA JOURNAL:

https://www.osapublishing.org/ol/abstract.cfm?uri=ol-45-13-3377

Optics Letters

In vivo time-domain diffuse correlation spectroscopy above the water absorption peak

L. Colombo,[1,*] M. Pagliazzi,[2] S. Konugolu Venkata Sekar,[1] D. Contini,[1] T. Durduran,[2,3] and A. Pifferi[1,4]

[1]Politecnico di Milano, Dipartimento di Fisica, 20133 Milano, Italy
[2]ICFO-Institut de Ciències Fotòniques, The Barcelona Institute of Science and Technology, 08860 Castelldefels (Barcelona), Spain
[3]Institució Catalana de Recerca i Estudis Avançats (ICREA), 08015 Barcelona, Spain
[4]Istituto di Fotonica e Nanotecnologie, Consiglio Nazionale delle Ricerche, 20133 Milano, Italy
*Corresponding author: lorenzo.colombo@polimi.it

Received 9 March 2020; revised 8 May 2020; accepted 9 May 2020; posted 12 May 2020 (Doc. ID 392355); published 17 June 2020

Time-domain diffuse correlation spectroscopy (TD-DCS) is a newly emerging optical technique that exploits pulsed, yet coherent light to non-invasively resolve the blood flow in depth. In this work, we have explored TD-DCS at longer wavelengths compared to those previously used in literature (i.e., 750–850 nm). The measurements were performed using a custom-made titanium-sapphire mode-locked laser, operating at 1000 nm, and an InGaAs photomultiplier as a detector. Tissue-mimicking phantoms and *in vivo* measurements during arterial arm cuff occlusion in $n = 4$ adult volunteers were performed to demonstrate the proof of concept. We obtained a good signal-to-noise ratio, following the hemodynamics continuously with a relatively fast (1 Hz) sampling rate. In all the experiments, the auto-correlation functions show a decay rate approximately five-fold slower compared to shorter wavelengths. This work demonstrates the feasibility of *in vivo* TD-DCS in this spectral region and its potentiality for biomedical applications.

https://doi.org/10.1364/OL.392355

Diffuse correlation spectroscopy (DCS) is an emerging optical technique that is able to non-invasively measure microvascular, deep-tissue (>1 cm deep) blood flow (BF) by monitoring the speckle fluctuations of coherent light diffused by biological tissue, which are characterized by their intensity auto-correlation function [1,2]. In a typical DCS experiment, light from a long coherence length (>1 m) continuous-wave (CW) laser is injected into the tissue and recollected, often in reflectance geometry, at a given source–detector (SD) separation (∼2−3 cm). Since the detected photons may undergo any possible path length in the tissue, depth resolution can be obtained only by using multiple SD separations or exploiting particular fitting algorithms [3]. Instead, if a pulsed, yet sufficiently coherent light source is used, it is possible to exploit the physical relationship between photon time of flight (TOF) and mean penetration depth [4,5] to recover depth resolution in the measured BF, this being the principle of an emerging technique called time-domain (TD) DCS [6–8].

TD-DCS for biomedical applications was first demonstrated experimentally on liquid phantoms and on small animals [7] by using narrow (few tens of picoseconds) temporal gates. Later, by means of broader (few nanoseconds) temporal gates, which enable a higher signal-to-noise ratio (SNR), the technique was extended to *in vivo* experiments on human muscle and brain [8,9]. Recently a hardware temporal gating scheme was also proposed, enabling quasi-null SD separation measurements [10]. Also, researchers have developed theoretical models for retrieving the BF from gated auto-correlation functions, taking into account heterogeneous geometries, finite coherence length, and the instrument response function (IRF) [11–13].

Very recently, the use of light sources with wavelength above the so-called water absorption peak (∼950 nm) was proposed to improve the SNR and penetration depth of CW- and TD-DCS [14,15]. This is based on theoretical considerations related to the physics of the light-tissue interactions at those longer wavelengths, but the limitations of the opto-electronics are the main hindrance in its practical implementation. In particular, in this spectral region due to the decrease in reduced scattering [16,17] and light wavenumber, the auto-correlation functions are expected to have a slower decay rate thus enabling longer correlation bin times and consequently a larger SNR [3]. In addition to that, for a given temporal gate, the penetration depth is proportional to the inverse of the reduced scattering coefficient [5], thus potentially increasing the depth sensitivity.

TD-DCS measurements above the water peak were already demonstrated in 1990 on phantoms, using a mode-locked Nd:YAG laser and an optical gating based on second-harmonic generation [6], an approach unsuitable for biomedical applications. In this paper, we explore TD-DCS in that spectral range, by exploiting the wide tunability of a custom-made pulsed, high-temporal coherence, active mode-locked Ti:sapphire laser operated above 1000 nm, reporting both phantom and *in vivo* measurements. The aim of this work is to show the feasibility of *in vivo* TD-DCS at longer than usual wavelengths and its potential impact in biomedical applications.

The experimental setup, which is a modified version of the one described in Ref. [8], is depicted in Fig. 1. Briefly, the Ti:sapphire (labeled in the figure with Ti:Sa) laser repetition

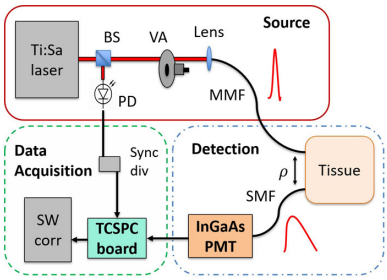

Fig. 1. Schematic of the experimental setup conceptually divided into three units: source (continuous line box), detection (dashed-dotted box), and data acquisition (dashed box).

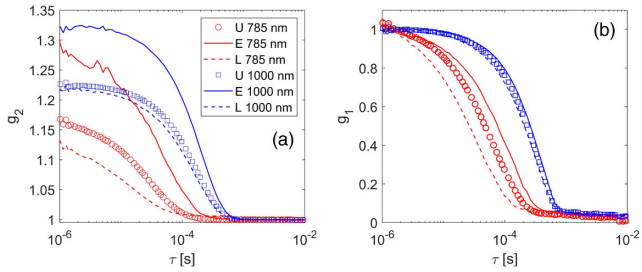

Fig. 2. Liquid phantom experiment: (a) ungated (U, symbols) early gate (E, continuous lines) and late gate (L, dashed lines) intensity auto-correlations $g_2(\tau)$ and (b) corresponding electric field auto-correlations $g_1(\tau)$, measured at $\lambda = 785$ nm (red curves) and 1000 nm (blue curves). For both wavelengths, 500 ungated and gated auto-correlation functions with a 1 s integration time each were averaged for a total of 500 s of acquisition.

frequency was 100 MHz and a set of cavity mirrors for operation between 900 nm and 1050 nm was used. We tuned the wavelength (λ) to 1000 nm, close to the maximum wavelength we achieved with the used 5 W pump laser, and the pulse width to approximately 200 ps for all experiments. Light was attenuated by means of a variable attenuator (VA) and coupled with a focusing lens to a 100 μm diameter graded-index multi-mode fiber (MMF) and sent to the surface of the sample. The diffused light was then recollected, at a SD separation $\rho = 1$ cm, with a 4.4 μm core diameter single-mode fiber (SMF) (780HP, Neufern) and delivered to an InGaAs photomultiplier tube (PMT) (H10330-25 Hamamatsu Photonics, Japan) bearing 2% quantum efficiency at 1000 nm and 400 ps time transit spread. For generating a synchronization signal (Sync), we placed a beam splitter (BS) and a photodiode (PD) (OCF-401, Becker & Hickl, Germany) at the output of the source. A time-correlated single-photon counting (TCSPC) board (Time Harp 260 pico, PicoQuant, Germany) was used for recording the absolute arrival time of each detected photon, as well as the delay from the Sync signal (so-called pulse time) with a 25 ps temporal resolution. For every photon, the absolute arrival time and pulse time, together, i.e., time stamps, are stored in a PC and post-processed with a software auto-correlator (SW corr) as described in Ref. [8].

Temporal gating is obtained via software, considering only photons with TOFs belonging to a specific temporal gate for calculation of the auto-correlation function. From the normalized intensity auto-correlation function $g_2(\tau)$, where τ is correlation delay time, the normalized electric field auto-correlation function $g_1(\tau)$ is obtained using the Siegert relation [18] $g_2(\tau) = 1 + \beta|g_1(\tau)|^2$, where β is a constant, equal to 0.5 for an ideal (i.e., infinite coherence length of the source) experiment with unpolarized, single-mode detection. The electric field auto-correlation function for sufficiently high source temporal coherence can be expressed as [12,13]

$$g_1(\tau) = \int_0^{+\infty} f(s)\mathrm{EGF}(s)\exp(-ks\tau)\mathrm{d}s\,, \qquad (1)$$

where $f(s)$ is the normalized distribution of photon path lengths s, estimated by the theoretical time-resolved diffuse reflectance normalized to unitary area. EGF is the so-called effective gate function, accounting for the effect of the IRF, which is defined as $\mathrm{EGF}(s) = \int_{s_0}^{s_0+\Delta s} \mathrm{IRF}(s'-s)\mathrm{d}s'$, where s_0 is the gate start, and Δs is the gate width. Finally, in Eq. (1), k is the auto-correlation decay rate per unit path length, equal to $2\mu_s' k_0^2 \alpha D_B$, where μ_s' is the reduced scattering coefficient, k_0^2 is the square of the light wavenumber in the medium, D_B is the Brownian diffusion coefficient of the scatterers, and α is the fraction of moving scatterers to total scatterers. The product αD_B is considered the BF index (BFI) of the tissue.

First, in order to characterize the system, we have performed a 500 s experiment using a homogenous tissue-mimicking liquid phantom prepared by adding 1% in mass of scatterers (Intralipid, B. Braun Melsungen, Germany) to distilled water [19]. An additional experiment was carried out at 785 nm, while keeping the same pulse width, using a single-photon avalanche diode detector (PDM, Micro Photon Devices srl, Italy) having a 15% quantum efficiency at that wavelength. The illumination power was set to 50 mW for all phantom experiments. The reduced scattering coefficient, as measured with a broadband time-resolved spectrometer, was $\mu_s' = 10\ \mathrm{cm}^{-1}$ and $\mu_s' = 7.4\ \mathrm{cm}^{-1}$ at 785 and 1000 nm, respectively. For *in vivo* measurements, ethical approval was obtained by Politecnico di Milano, and four adult subjects were recruited. A soft black probe with source and detector fibers was placed on the brachioradialis muscle of the subject's left arm, attenuating the laser power to 30 mW. The thickness of the superficial tissue layer above the muscle was estimated with a plicometer. A standard arm cuff was placed above the position of the probe. Data were acquired for 3 min (rest/baseline) followed by the occlusion of the tourniquet (200 mmHg pressure) for another 3 min. Finally, the recovery of the BF was followed after a rapid deflation for 4 min.

Regarding the phantom experiments, in Fig. 2, we compare the intensity and electric field auto-correlations, $g_2(\tau)$ and $g_1(\tau)$, respectively, measured at the two different wavelengths 785 and 1000 nm for ungated acquisition, an early gate and a late gate. The count rate was, respectively, 639 ± 2 kcps (mean $\pm$ Std Dev) and 249 ± 3 kcps for the 785 nm (red curves) and 1000 nm (blue curves) experiments. As can be seen in Fig. 2(a), moving from $\lambda = 785$ nm to 1000 nm, the intensity auto-correlation functions show a larger amplitude and a slower decay rate, for both ungated and gated acquisition. In particular [see Fig. 2(b)], the electric field ungated auto-correlation decay time [i.e., point where $g_1(\tau)$ falls below 0.5] moves from 45 ± 2 μs to 217 ± 16 μs, almost five times slower. This effect is a combination of changes in the light wavenumber (k_0) and in the optical properties and is expected to hold also *in vivo* (see below). It may be noted, in particular, that only the term

$\mu_s' k_0^2$ in the exponential part of $g_1(\tau)$ contributes to reduce the decay rate by a factor of 2.2. Nevertheless, the measured D_B was $(1.0 \pm 0.1) \cdot 10^{-8}$ cm^2/s and $(0.97 \pm 0.04) \cdot 10^{-8}$ cm^2/s at 785 and 1000 nm, respectively, showing no statistically significant variation.

Conversely [see Fig. 2(a)], the β parameter (value of the intensity auto-correlation at zero delay time) is increased from 0.16 to 0.22, a relatively high value for pulsed lasers, and we believe this is due to the change in optical properties. In fact, the reduction in the reduced scattering and increase in the absorption coefficients narrow the path length distribution, increasing the probability for the detected photons to have path length differences smaller than the laser coherence length, which increases the degree of interference [20]. For further details about the relationship among beta, laser coherence length, and gate position, see Ref. [12].

The cuff occlusion experiments were performed on $n = 4$ adult subjects (30–53 years old, all male). Their superficial layer thickness, in the position of the optical probe, is reported in Table 1. To obtain accurate values for the baseline optical properties, we scanned the subjects while lying at rest with the laboratory version of the broadband time-resolved diffuse optical spectrometer described in Ref. [21] with a SD separation $\rho = 1$ cm. Table 1 reports the measured absorption (μ_a) and reduced scattering coefficients (μ_s') at 785 and 1000 nm. As can be seen, for both wavelengths the optical properties show a high inter-subject variability, especially in the absorption coefficient. In fact, for subjects with a thinner superficial layer, the measured μ_a tends to be higher, due most probably to an increased sensitivity to the deeper muscle layer, which typically has a higher water and hemoglobin content [17].

In the following, we report the results of the cuff occlusion experiments. For each subject, the average count rate during the 1000 nm experiment is reported in Table 1. The full-width at half maximum (FWHM) of the distribution of TOFs (DTOF) curves was 468 ± 12 ps. We have computed, with a 1 s sampling time, the auto-correlation functions considering two temporal gates: an early gate, starting when the DTOF emerged from the noise floor and ending at 50% of its maximum value on the rising edge side only, and a late gate, starting at $t = 400$ ps and ending at $t = 1$ ns, with $t = 0$ ps set at the IRF peak. At the late gate starting time, the DTOF curves fell below $41 \pm 13\%$ of their maximum values. Figure 3(a) compares the intensity auto-correlation functions $g_2(\tau)$ measured in the experiments at 785 and 1000 nm (red and blue curves, respectively) for the early (E) and late gate (L), during the baseline condition (for subject 1, 5 s average).

In Fig. 3(b), we compare the late gate electric field auto-correlation functions [$g_1(\tau)$] measured at 1000 nm and their fits (continuous lines) at three phases of the protocol: baseline (red triangles), during the occlusion (green diamonds), and 10 s after the occlusion release, in correspondence of the hyperemic peak (blue circles). All the fits were performed considering the region from $\tau = 10^{-5} s$ to the point where $g_1(\tau)$ fell below 0.5. As in the case of the phantom experiment, for both early and late gates, the auto-correlation functions at 1000 nm show a decay rate approximately five times slower compared to the corresponding curves measured at 785 nm.

The value of the β parameter [see Fig. 3(a)] depends on the gate position and is equal to 0.37 and 0.24, respectively, for the early and late gates, for the 1000 nm experiment. Figure 3(b)

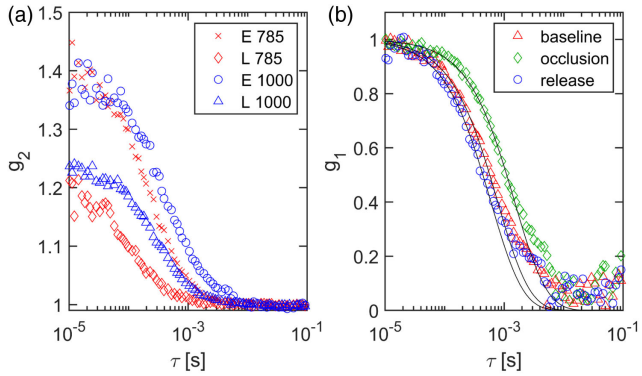

Fig. 3. Cuff occlusion experiment auto-correlation functions, 5 s averaging time. The data shown refer to subject 1. (a) Baseline intensity auto-correlations for early gate (E) and late gate (L) measured at 785 nm (red crosses and diamonds) and 1000 nm (blue circles and triangles). (b) For the 1000 nm experiment, late gate electric field auto-correlations (symbols) and fits (black lines) measured at baseline (red triangles), during occlusion (green diamonds) and 10 s after the occlusion release (blue circles).

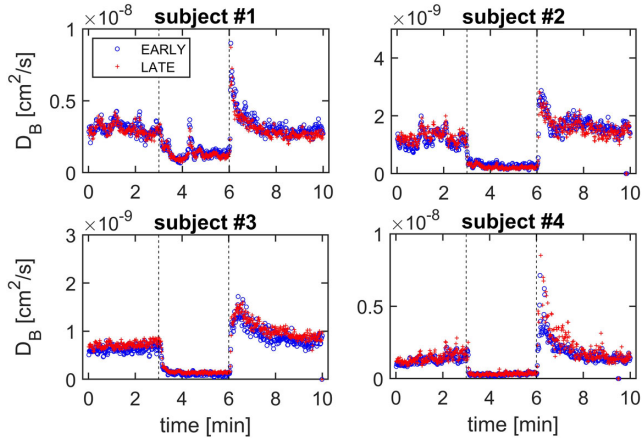

Fig. 4. BFI temporal traces measured during the cuff occlusion experiments at 1000 nm from the early (blue circles) and late gate (red crosses) auto-correlation data. The occlusion initial and final times at minute 3 and 6, respectively, are marked by the vertical dashed lines. Note that different y axes limits are used in the different panels.

demonstrates the sensitivity of the late gate auto-correlation function to hemodynamic changes, for the 1000 nm wavelength. In particular, the $g_1(\tau)$ decay rate changes significantly when moving from baseline to cuff occlusion and to the subsequent release, which corresponds to the hyperemic peak induced by the decrease in oxygen supply during the occlusion. Distortions of the data from the theoretical model at long delay times, appearing outside the fitting region, are common in *in vivo* DCS and can be an effect of tissue heterogeneity [2].

Finally, in Fig. 4, we report for each subject the retrieved BFI traces with a sampling time of 1 s from the early and late gate auto-correlation functions measured at 1000 nm (blue circles and red crosses, respectively). In Table 1, we report for the 1000 nm experiments the baseline BFI for the early and late gates and ungated acquisition, which were retrieved by averaging the first 3 min of the experiment for a total of

Table 1. *In vivo* Experiment: Superficial Tissue Thickness, Optical Properties, Average Count Rate, and Baseline BFI for Each of the Four Subjects[a]

	Superficial Thickness	μ_a [cm^{-1}]	μ_s' [cm^{-1}]	μ_a	μ_s'	Count Rate	D_B [10^{-9} cm^2/s] 1000 nm			D_B 785 nm
Subject	[mm]	785 nm		1000 nm		[kcps]	Early	Late	Ungated	Ungated
1	2.7	0.24	9.3	0.52	7.7	151 ± 3	3.1 ± 0.4	3.0 ± 0.4	3.0 ± 0.36	3.6 ± 0.38
2	4.8	0.13	9.4	0.25	7.9	263 ± 9	1.2 ± 0.24	1.3 ± 0.2	1.1 ± 0.2	0.74 ± 0.09
3	6.5	0.12	10.4	0.22	8.9	336 ± 7	0.63 ± 0.07	0.72 ± 0.06	0.59 ± 0.05	1.5 ± 0.13
4	2.2	N/A	N/A	0.49	7.8	112 ± 11	1.2 ± 0.25	1.3 ± 0.31	1.2 ± 0.2	N/A

[a]Below each parameter, we specify the measured wavelength. The count rate refers to the 1000 nm experiment.

180 time points. The BFI tends to be higher for the late gate compared to the early gate, suggesting that the later photons indeed probe deeper, more oxygen-consuming, tissues such as muscles, compared to shallower ones, such as skin and fat. The limited superficial thickness may hinder BF differences in the different tissue layers. Also, the baseline values of the ungated BFI from the experiments at 1000 nm are comparable, within a factor of two, to the ungated BFI measured at 785 nm (reported in Table 1, last column). The BFI differences at the two wavelengths may be due to the probe repositioning or slight physiological changes between the two measurements.

Regarding the temporal trend, as can be seen in Fig. 4, the BFI has the expected temporal profile for both temporal gates in all the measured subjects. In particular, the BFI drops significantly in correspondence with the cuff occlusion (min 3), and after the release (min 6), it overshoots to a hyperemic value much larger than the baseline BFI, as expected by physiology and previous works at shorter wavelengths. It may be noted that the tissue absorption in this spectral range is large (see Table 1), due to the proximity of the water absorption peak [17]. This reduces the relative number of later, deeply probing, photons compared to earlier ones. However, moving to even longer wavelengths such as 1050–1100 nm, the water absorption contribution would decrease strongly, thus enhancing the achievable depth sensitivity albeit with the need for a higher pump laser power or a different active medium.

In this paper, we have reported a novel TD-DCS experimental setup for operation above the water absorption peak ($\lambda > 950$ nm). The setup is based on a tunable mode-locked Ti:sapphire laser source and an InGaAs photomultiplier. We have reported TD-DCS measurements at 1000 nm, on both liquid phantoms and four volunteers following an arterial, arm cuff-occlusion protocol. In both cases, we have observed an approximately five-fold slower auto-correlation decay rate, which may result in improved SNR and also, due to the lower scattering, larger depth sensitivity. In order to apply the technique in clinical environments, we envision the use of a more compact laser source, with an even higher operational wavelength and more efficient detectors to reduce system complexity and increase throughput.

Funding. Horizon 2020 Framework Programme (LASERLAB-EUROPE V (n. 871124), LUCA (n. 688303, H2020-ICT-2015)).

Disclosures. The authors declare no conflicts of interest.

REFERENCES

1. D. A. Boas and A. G. Yodh, J. Opt. Soc. Am. A **14**, 192 (1997).
2. T. Durduran, R. Choe, W. B. Baker, and A. G. Yodh, Rep. Prog. Phys. **73**, 076701 (2010).
3. C. Zhou, G. Yu, D. Furuya, J. H. Greenberg, A. G. Yodh, and T. Durduran, Opt. Express **14**, 1125 (2006).
4. A. Pifferi, D. Contini, A. Dalla Mora, A. Farina, L. Spinelli, and A. Torricelli, J. Biomed. Opt. **21**, 091310 (2016).
5. L. Spinelli, A. Farina, T. Binzoni, A. Torricelli, A. Pifferi, and F. Martelli, Sci. Rep. **6**, srep27057 (2016).
6. A. G. Yodh, P. D. Kaplan, and D. J. Pine, Phys. Rev. B **42**, 4744 (1990).
7. J. Sutin, B. Zimmerman, D. Tyulmankov, D. Tamborini, K. C. Wu, J. Selb, A. Gulinatti, I. Rech, A. Tosi, D. A. Boas, and M. A. Franceschini, Optica **3**, 1006 (2016).
8. M. Pagliazzi, S. K. V. Sekar, L. Colombo, E. Martinenghi, J. Minnema, R. Erdmann, D. Contini, A. Dalla Mora, A. Torricelli, A. Pifferi, and T. Durduran, Biomed. Opt. Express **8**, 5311 (2017).
9. D. Tamborini, K. A. Stephens, M. M. Wu, P. Farzam, A. M. Siegel, O. Shatrovoy, M. Blackwell, D. A. Boas, S. A. Carp, and M. A. Franceschini, IEEE Trans. Biomed. Eng. **66**, 3014 (2019).
10. M. Pagliazzi, S. K. Sekar, L. Di Sieno, L. Colombo, T. Durduran, D. Contini, A. Torricelli, A. Pifferi, and A. Dalla Mora, Opt. Lett. **43**, 2450 (2018).
11. J. Li, L. Qiu, C.-S. Poon, and U. Sunar, Biomed. Opt. Express **8**, 5518 (2017).
12. X. Cheng, D. Tamborini, S. A. Carp, O. Shatrovoy, B. Zimmerman, D. Tyulmankov, A. Siegel, M. Blackwell, M. A. Franceschini, and D. A. Boas, Opt. Lett. **43**, 2756 (2018).
13. L. Colombo, M. Pagliazzi, S. K. V. Sekar, D. Contini, A. Dalla Mora, L. Spinelli, A. Torricelli, T. Durduran, and A. Pifferi, Neurophotonics **6**, 035001 (2019).
14. D. Tamborini, V. Anant, B. A. Korzh, M. D. Shaw, S. A. Carp, and M. A. Franceschini, in *Biophotonics Congress: Optics in the Life Sciences Congress* (2019), paper BW1A.5.
15. M. A. Franceschini, S. A. Carp, D. Tamborini, D. A. Boas, B. R. Rosen, M. Blackwell, and O. Shatrovoy, WO/2019/161336 (2019).
16. P. Taroni, A. Bassi, D. Comelli, A. Farina, R. Cubeddu, and A. Pifferi, J. Biomed. Opt. **14**, 054030 (2009).
17. S. L. Jacques, Phys. Med. Biol. **58**, 5007 (2013).
18. P.-A. Lemieux and D. J. Durian, J. Opt. Soc. Am. A **16**, 1651 (1999).
19. L. Cortese, G. L. Presti, M. Pagliazzi, D. Contini, A. Dalla Mora, A. Pifferi, S. K. V. Sekar, L. Spinelli, P. Taroni, M. Zanoletti, and U. M. Weigel, Biomed. Opt. Express **9**, 2068 (2018).
20. T. Bellini, M. A. Glaser, N. A. Clark, and V. Degiorgio, Phys. Rev. A **44**, 5215 (1991).
21. S. K. V. Sekar, A. Dalla Mora, I. Bargigia, E. Martinenghi, C. Lindner, P. Farzam, M. Pagliazzi, T. Durduran, P. Taroni, A. Pifferi, and A. Farina, IEEE J. Sel. Top. Quantum Electron. **22**, 406 (2016).